Dynamic Estimation of Cardiovascular State from Arterial Blood Pressure Recordings

Taylor E. Baum, Elie Adam, Christian S. Guay, Gabriel Schamberg, Mohammadreza Kazemi, Thomas Heldt, and Emery N. Brown

***Abstract*— Real-time estimation of patient cardiovascular states, including cardiac output and systemic vascular resistance, is necessary for personalized hemodynamic monitoring and management. Highly invasive measurements enable reliable estimation of these states but increase patient risk. Prior methods using minimally invasive measurements reduce patient risk but have produced unreliable estimates limited due to trade-offs in accuracy and time resolution. Our objective was to develop an approach to estimate cardiac output and systemic vascular resistance with both a high time resolution and high accuracy from minimally invasive measurements. Using the two-element Windkessel model, we formulated a state-space method to estimate a dynamic time constant – the product of systemic vascular resistance and compliance – from arterial blood pressure measurements. From this time constant, we derived proportional estimates of systemic vascular resistance and cardiac output. We then validated our method with a swine cardiovascular dataset. Our estimates produced using arterial blood pressure measurements not only closely align with those using highly invasive measurements, but also closely align when derived from three separate locations on the arterial tree. Moreover, our estimates predictably change in response to standard cardiovascular drugs. Overall, our approach produces reliable, real-time estimates of cardiovascular states crucial for monitoring and control of the cardiovascular system.**

***Index Terms*— Arterial blood pressure, cardiac output, estimation, state-space, systemic vascular resistance, Windkessel model.**

I. Introduction

REAL-TIME monitoring of a patient's cardiovascular system in the operating room (OR) and intensive care unit (ICU) is necessary for personalized hemodynamic management. Poorly managed perioperative hypotension (low blood pressure) and hypertension (high blood pressure) can lead to severe postoperative organ dysfunction [1]–[4]. Hypotension or hypertension can originate from changes in systemic vascular resistance (R), cardiac output (CO) or some combination of both [5]–[8]. Despite similar effects on blood pressure, changes in R or CO require different treatments. For example, a decrease in resistance to blood flow (R) leads to hypotension and treatment requires vasoconstrictors. A decrease in the amount of blood pumped from the heart (CO) also leads to hypotension while treatments require either positive inotropic drugs, intravenous fluid boluses or interventions to relieve obstruction of blood flow into or out of the heart. Selecting the incorrect treatment can have severe consequences. For example, treating hypotension due to heart failure with pure vasoconstrictors can further decrease cardiac output and worsen end-organ perfusion. It then becomes essential to monitor R and CO in real time for appropriate hemodynamic management.

The cardiovascular states R and CO can only be measured directly using highly invasive techniques. The most common measurement method, thermodilution, requires a pulmonary artery catheter placed into the heart [9]. This intervention greatly increases risks of bleeding, infection, arrythmias, tricuspid valve damage, right ventricular perforation and pulmonary artery rupture [10]. Such risks often render the collection of highly invasive measurements clinically unsuitable [11], [12]. As a result, estimation methods using minimally invasive measurements have been proposed [13]–[18]. Some prior methods use arterial blood pressure (ABP) and the two-element Windkessel model [19] to estimate R and CO from a dynamic time constant: $\tau = RC$ where C is arterial compliance [13]–[16]. However, these prior methods are limited due to trade-offs in time resolution and accuracy of τ estimates. For example, Simon et al. estimated τ through a simple exponential fit to the diastolic decay of each ABP pulse [13]. With this method, they achieved beat-by-beat resolution but sacrificed accuracy. Others sought to improve accuracy by incorporating a longer segment of ABP into a single estimate but sacrificed time resolution as a result [14]–[16]. Some of these prior methods then used their τ estimates to derive proportional estimates of CO [14]–[16]. These estimates are limited even further due to simplifying assumptions that disregard the full dynamics of the two-element Windkessel model. Overall, such methods – and methods using minimally invasive observations in general – produce unreliable estimates [20], [21], resulting in conflicting support for their clinical use [22], [23].

Using the two-element Windkessel model, we developed an approach that addresses the above limitations and allows us to

This work was supported by the NSF GRFP (1122374) and a Mathworks Fellowship to T. E. Baum, and by the Picower Institute, the NIH Award R01-NS123120 from NINDS and generous support from the JPB Foundation to E. N. Brown.

T. E. Baum, and T. Heldt are with the Department of Electrical Engineering and Computer Science, Massachusetts Institute of Technology, MA, USA

T. E. Baum, E. Adam, C. S. Guay, G. Schamberg and E. N. Brown are with the Picower Institute for Learning and Memory, Massachusetts Institute of Technology, MA, USA

E. Adam, C. S. Guay, G. Schamberg and E. N. Brown are with the Department of Anesthesia, Critical Care and Pain Medicine, Massachusetts General Hospital, MA, USA

M. Kazemi is with Department of Electrical and Computer Engineering, Florida International University, FL, USA

E. N. Brown is with Department of Anaesthesia, Harvard Medical School, MA, USA

Corresponding authors are T. E. Baum and E. N. Brown (e-mail: tbaum@mit.edu, enb@neurostat.mit.edu)

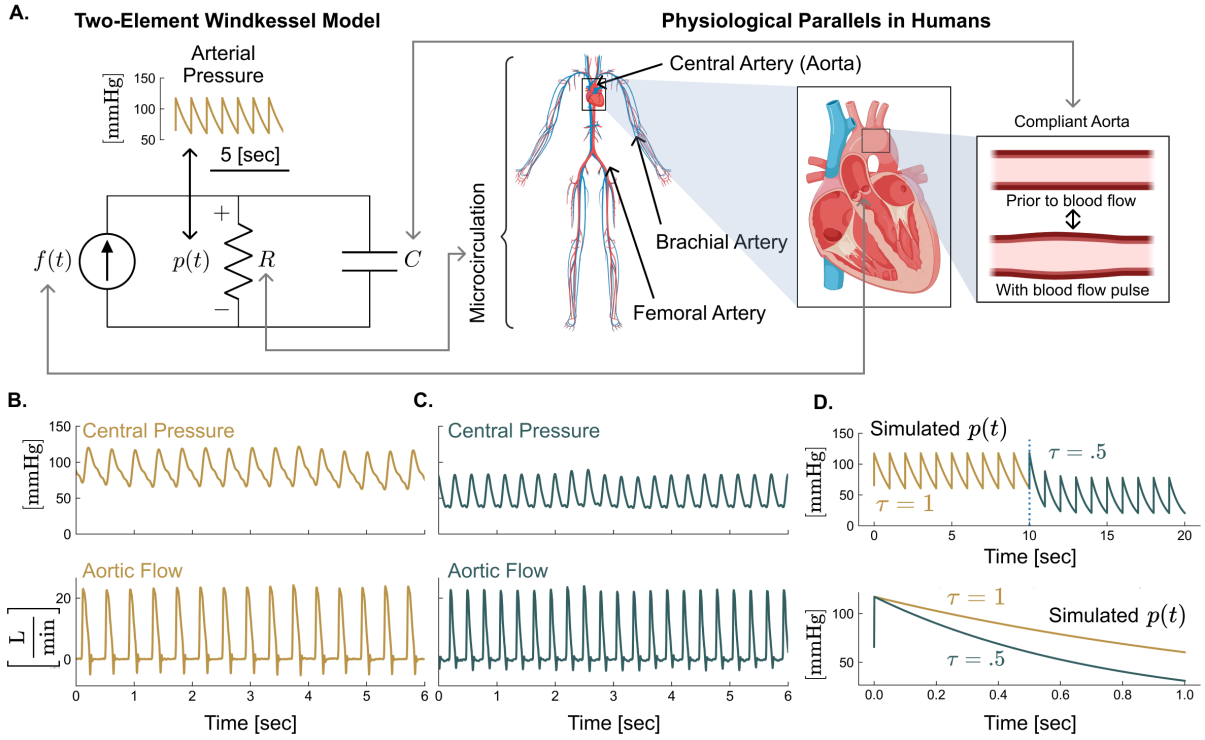

Fig. 1. **Illustration of Physiological Model. A.** The two-element Windkessel model, which models arterial blood pressure (ABP) as an RC-circuit receiving blood flow from the heart, and its physiological parallels in humans [24]. Components of this model include aortic flow (AF) into the system as $\boldsymbol{f(t)}$, ABP as $\boldsymbol{p(t)}$, arterial resistance from the microcirculation as R and compliance of large arteries, with primary contributions from the aorta, as C. The time constant of this model is $\boldsymbol{\tau = RC}$. We highlight three locations of arterial catheterization (femoral, brachial and central), as analog locations were used in the experimental swine dataset. **B.** *In vivo* swine central ABP (top) and AF (bottom) with $\tau \approx 1$. **C.** *In vivo* swine central ABP (top) and AF (bottom) with $\tau \approx .5$. **D.** (top) Simulation of the Windkessel Model forward in time with $\boldsymbol{R = 1}$ and $\boldsymbol{C = 1}$ from $\boldsymbol{0 \leq t < 10}$ and then $\boldsymbol{C = 1}$ and $\boldsymbol{R = .5}$ from $\boldsymbol{10 \leq t < 20}$ where $\boldsymbol{t}$ is time. (bottom) Comparison of the exponential decay of one beat for $\boldsymbol{C = 1}$ and $\boldsymbol{R = 1}$ (light green) versus $\boldsymbol{C = 1}$ and $\boldsymbol{R = .5}$ (dark green).

estimate R and CO proportionally in real time. This approach avoids independence assumptions (i.e., that R and C are not dynamically interlinked) through use of the full dynamics of the two-element Windkessel model. First, using ABP, we developed a method to estimate proportional R (τ). We achieved this by constructing a state-space model of τ, with τ as the state and the diastolic component of each ABP pulse as observations. Our method improves upon previous techniques by producing beat-by-beat estimates of τ with reduced noise through incorporation of ABP history outside of the current beat. Second, also using ABP, we developed a method to estimate proportional CO (CO/C). This method combines the estimates of proportional R into another state-space model that also achieves beat-by-beat estimates with reduced noise. Third, using aortic flow (AF) and ABP, we developed a method to estimate R and C separately. From this, we have direct measurements of CO from AF and estimates of R and C. These more-informed estimates were used for comparison to our proportional R and CO estimates from ABP.

Through application of our approach to a previously collected swine dataset [14], we find three major results. First, we find that our minimally invasive proportional R and CO estimates align with our highly invasive estimates using ABP and AF for each swine and each location. Second, we find that our proportional R and CO estimates within a swine often align across multiple ABP recording locations, emphasizing the conservation of these states throughout the arterial tree. Third, we find that our proportional R and CO estimates respond predictably to commonly used cardiovascular drugs. As validated with swine data, we provide improved methods to estimate clinically integral cardiovascular states describing vascular and cardiac function.

Paper structure: In Section II, we present our results as a sequence of methodological developments and subsequent findings from applying our methods to a previously collected swine dataset. In Section III, we discuss the benefits and limitations of our approach along with this work's clinical implications. In Section IV, we conclude this paper. In the Appendix, we present the materials and methods of this work in full mathematical detail. In the Supplementary Information are additional details.

II. Results

A. A cardiovascular state can be characterized independently of its location on the arterial tree by the time constant of a circuit model of the cardiovascular system

We built on the two-element Windkessel model [19] to characterize a cardiovascular state from arterial blood pressure dynamics. In Figure 1A, we illustrate the circuit representation of the two-element Windkessel model and its physiological parallels in humans. This model represents the cardiovascular system through two main mechanistic components: R and C.

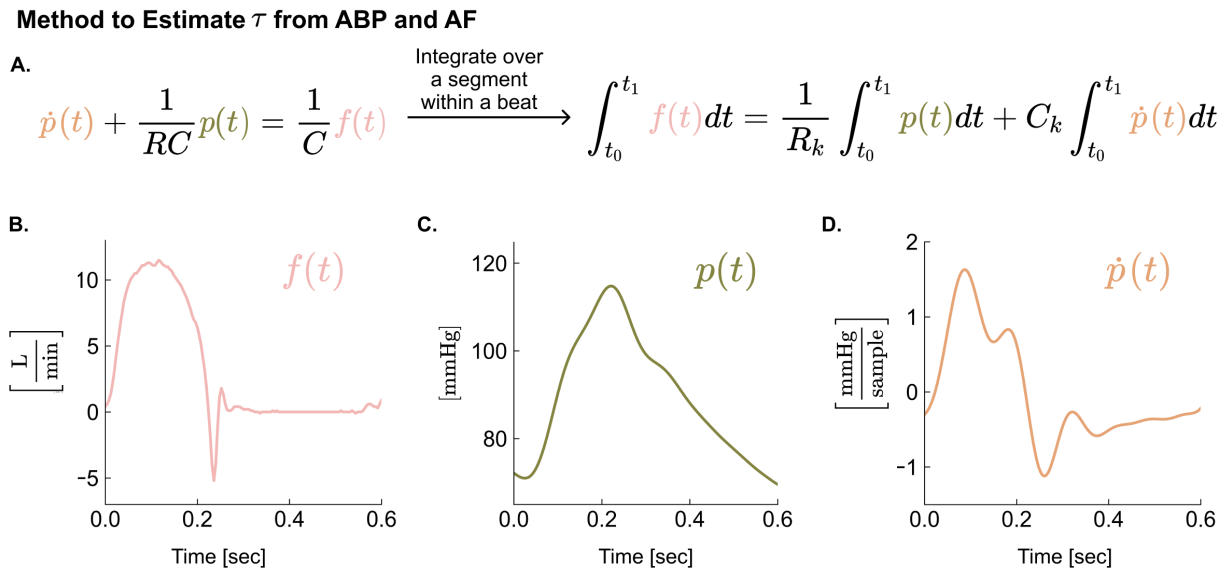

Fig. 2. **Method to Estimate τ from Aortic Flow (AF) and Arterial Blood Pressure (ABP). A**. We used the dynamic equation from the two-element Windkessel model to generate estimates of τ using AF, ABP and an approximate derivative of pressure. **B**. Example *in vivo* swine AF ($\boldsymbol{f(t)}$). **C**. Example *in vivo* swine ABP ($\boldsymbol{p(t)}$). **D**. Example *in vivo* derivative of swine ABP ($\boldsymbol{\dot{p}(t)}$).

The C component represents elasticity of the blood vessels, with primary contributions from the walls of major arteries. The R component represents the forces opposing blood flow, with major contributions from the arterial microcirculation (i.e., arterioles, capillaries and venules). Both of these contribute to arterial pressure, and the two-element Windkessel model captures their contribution by an RC circuit.

A pulse of blood volume (Fig. 1B,C bottom) into this RC model immediately meets a vascular resistance that opposes that flow. This inflates the vessels and engages their compliance (i.e., capacitance). The compliant vessels then push this flow through the vascular resistance, giving rise to blood pressure (i.e., voltage drop across the resistor). This pressure decays with time as blood crosses from arteries to veins (Fig. 1B,C top). The two-element Windkessel model describes this decay in blood pressure as exponential with a rate governed by τ (Fig. 1D). We used this time constant as the cardiovascular state to estimate. Changes in τ directly modulate blood pressure. One can formalize this relationship with a differential equation (Eq. 1) whose solution is a model of blood pressure:

$$\dot{p}(t) + \frac{1}{RC}p(t) = \frac{1}{C}f(t) \tag{1}$$

where $f(t)$ in $[\mathrm{L}\cdot\mathrm{min}^{-1}]$ is the volumetric inflow into the blood vessels from the heart, $p(t)$ in [mmHg] is blood pressure, C is in $[\mathrm{L}\cdot\mathrm{mmHg}^{-1}]$ and R is in $[\mathrm{mmHg}\cdot\mathrm{min}\cdot\mathrm{L}^{-1}]$.

The two-element Windkessel model is often described to model blood pressure in the aorta. To estimate τ peripherally, we extended the two-element Windkessel model to incorporate peripheral vasculature (Fig. S1). While R and C can change along the arterial tree, we find that, under reasonable assumptions (see Supplementary Information, Sec. A) τ is preserved throughout. Our finding suggests that τ is a global cardiovascular state.

B. The time constant (proportional resistance) can be estimated using aortic flow and arterial blood pressure

We developed a method to estimate τ using ABP and highly invasive measurements of AF. Our method separately estimates R and C to get $\tau = RC$ as illustrated in Figure 2. Previous work describes common procedures to separately estimate R and C using insight from the two-element Windkessel model at every beat k [14], [16], [25]. In this prior work, compliance is computed as stroke volume (i.e., amount of blood volume pumped from the heart) over pulse pressure (i.e., difference between systolic and diastolic pressure) for each pulse:

$$C_k = \frac{\int_{o_k}^{o_k+T_f} f(t)dt}{\int_{o_k}^{o_k+T_f} \dot{p}(t)dt} \tag{2}$$

where o_k is the time of onset of the blood pressure pulse in [sec] and T_f is the duration of systole (i.e., positive flow from the heart) in [sec]. Also in this prior work, resistance is computed as the mean pressure divided by the average aortic flow for the k-th pulse:

$$R_k = T_k^{-1}\int_{o_k}^{o_k+T_k} p(t)dt \cdot \left(T_k^{-1}\int_{o_k}^{o_k+T_k} f(t)dt\right)^{-1} \tag{3}$$

where T_k is the period of the heart beat in [sec]. Systemic vascular resistance and compliance are interlinked, however, as dictated by the two-element Windkessel model. As such, an estimate of R and C using this approach leads to an erroneous result.

Instead, to estimate R and C together, we integrated Equation 1 over integration period t_0 to t_1, yielding:

$$\int_{t_0}^{t_1} f(t)dt = \frac{1}{R_k}\int_{t_0}^{t_1} p(t)dt + C_k\int_{t_0}^{t_1} \dot{p}(t)dt \tag{4}$$

By integrating over two periods within beat k – the entire pulse and the systolic period – we have two equations. The solution to

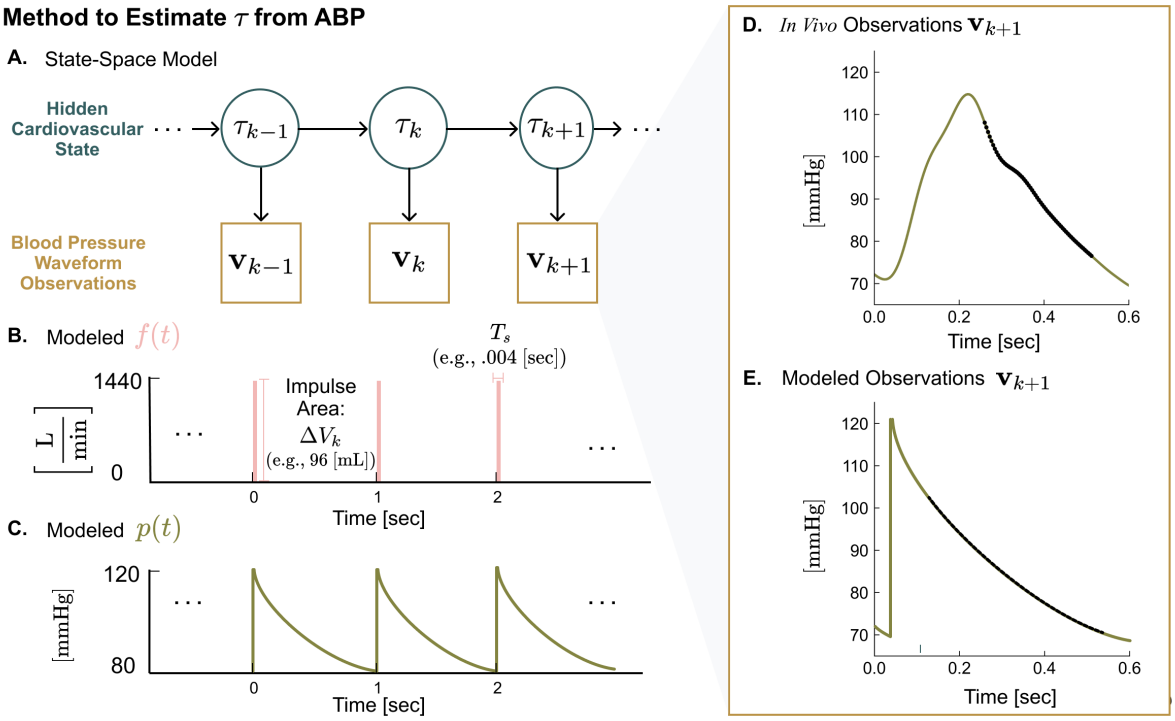

Fig. 3. **Method to Estimate τ from Arterial Blood Pressure (ABP).** We built a graphical model of τ in relation to samples of ABP and then built a Kalman filter around this model to learn τ at each beat k. **A.** Modeled ABP from the two-element Windkessel Model. **B.** Modeled aortic flow as impulses of stroke volume, ΔV_k. **C.** Graphical model of τ_k related to ABP ($p(t)$) observations, $\mathbf{v}_k$. **D.** Example *in vivo* ABP observations. **E.** Modeled ABP observations. We built a Kalman filter, constructed from two-element Windkessel model assumptions, to get an estimate of τ_k from the observations from each beat.

these two equations provides beat-by-beat estimates of R, C and, subsequently, $\tau = RC$ that are dynamically sound with respect to the two-element Windkessel model.

Notice, if we set the integration bounds to be over the full beat in Equation 4 and we set $R = 0$, we get Equation 2. With the same integration bounds, if we set $C = 0$, we get Equation 3.

C. Proportional resistance can be estimated using arterial blood pressure only

We developed a state-space method to estimate τ using only ABP. Our method (Fig. 3A) consists of a single hidden state (i.e., the time constant, τ) that is evolving with time, as described by our state equation. We estimate this hidden state from ABP observations, as described by our observation equation.

As flow into the aorta stops during the diastolic period (Fig. 3B), we expect a decay with a rate defined by the time constant, τ, which follows the dynamics of the two-element Windkessel model (Fig. 3C). We formalize this relation between the hidden cardiovascular state of interest, τ_k, and observations of the ABP waveform during diastole, $\mathbf{v}_k$, as:

$$\mathbf{v}_k = a_k \exp\left(-\frac{\mathbf{t}_k}{\tau_k}\right) \tag{5}$$

where k indexes the heart beats and $\mathbf{t}_k$ corresponds to the time value in [sec] elapsed from the first diastolic ABP observation. Additionally, we assumed a_k to be the initial observation of $\mathbf{v}_k$ (Fig. 3D,E).

We derive a set of linear observation equations for every pulse from Equation 5 (as detailed in the Appendix) and incorporate noise. We design this noise such that our confidence in observations at the beginning of the pulse decay is less. This is because our observation model assumes an absence of flow into the arterial vasculature during diastole, and flow is often non-zero around the closure of the aortic valve (Fig. 2B). Additionally, there is evidence that the influence of wave reflection on the shape of ABP pulses is smallest at end-diastole and early systole [26]–[28].

The hidden state, τ, is not fixed and is expected to vary as a function of time. As such, we assumed that τ_k follows a Gaussian random walk:

$$\tau_{k+1} = \tau_k + \eta_k \tag{6}$$

where $\eta_k \sim N(0, \sigma_\eta^2)$ and each η_k is independent. The state noise variance, σ_η^2, defines how quickly τ_k can change.

To obtain a real-time estimate of τ from ABP, we implemented a Kalman filter using Equation 5 as our observation equation and Equation 6 as our state equation. Our approach enables us to obtain a maximum a posteriori τ_k estimate, $\tau_{[k|k]}$, for every beat which incorporates prior history using minimally invasive ABP observations. The mathematical details of our algorithm are provided in the Appendix.

D. Proportional resistance estimates using arterial blood pressure are beat-by-beat with reduced noise

Our estimation method using ABP produces a smooth trajectory of beat-by-beat estimates of τ, where each beat estimate has an explicit credibility interval. Our algorithm takes an ABP segment as input (Fig. 4A, top) and provides an estimated τ

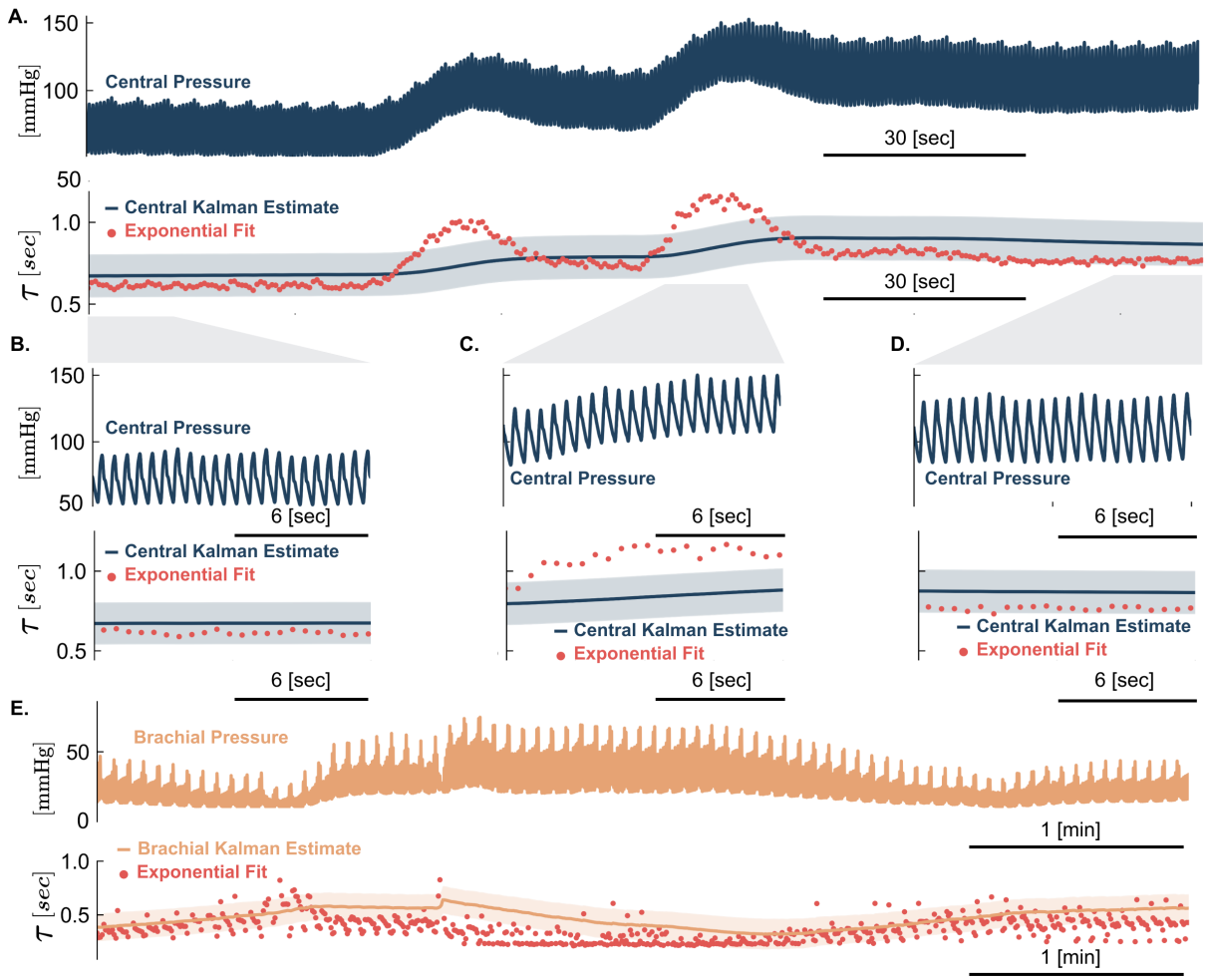

Fig. 4. **Benefits of Kalman Filter for Estimation of τ. A.** (top) Segment of central ABP waveform from experiment 1. (bottom) Corresponding Kalman τ estimates, along with exponential fit τ estimates lacking history dependence. **B.** Zoomed in segment of A. emphasizing Kalman τ estimates' resistance to breathing artifacts with $\tau \approx .6$. **C.** Zoomed in segment of A. emphasizing Kalman τ estimates' responsiveness to rapid changes. **D.** Zoomed in segment of A. emphasizing Kalman τ estimates' resistance to breathing artifacts with $\tau \approx .8$. **E.** (top) Segment of brachial ABP with potential prominent backward reflected pressure waves from experiment 2. (bottom) Corresponding Kalman τ estimates, along with exponential fit τ estimates lacking history dependence.

trajectory (Fig. 4A, bottom). We compare this to τ estimates obtained independently at each beat (Fig. 4A, bottom, in red) by fitting an exponential curve to the diastolic portion of each ABP pulse. A standard exponential fit is a natural first approach to estimate τ [13] but is highly susceptible to noise and assumes equal confidence in all ABP samples.

Due to our observation equation noise design (which we argue is more appropriate in Section IIC), our Kalman filter performs a different computation than smoothing a standard exponential fit. This can lead to an observed bias where our Kalman estimates do not track the center of standard exponential fits during stable periods (Fig. 4A, bottom, final 60 seconds). We emphasize that this bias is not equivalent to poor performance, and there would not be such a bias when comparing our Kalman estimates to exponential fits with our same noise assumption.

We find that our Kalman estimates are responsive to quick changes in τ (Fig. 4C). We emphasize that the sensitivity of τ estimates to rapid changes can be tuned by adjusting the model's noise terms. We also find that by incorporating history dependence, our algorithm filters out noise artifacts related to breathing (observe the oscillations in the red trajectory in Figure 4A-D) or prominent backward reflected pressure waves in peripheral catheters [26]–[28] (observe the variance in exponential fits in Figure 4E). This leads to a smooth state estimate trajectory (Fig. 4A-E).

In general, our Kalman estimates improve upon standard exponential fits by amplifying the general changes of τ, emphasizing ABP observations we are more confident in and minimizing the noise present in these ABP observations.

E. Proportional resistance estimates using arterial blood pressure track estimates using additional aortic flow measurements

The time constant, $\tau = RC$, can be estimated from ABP and AF by separately computing R and C using the two-element Windkessel model dynamics (Fig. 2). Our state-space method (Fig. 3) enables us to estimate τ from just ABP, bypassing the use of highly invasive AF measurements. It then remains to check whether τ estimates derived with ABP agree with those derived with ABP and AF. As such, we applied both methods to a previously collected swine dataset with six swine and compared the resultant τ estimates. For each swine, we produced

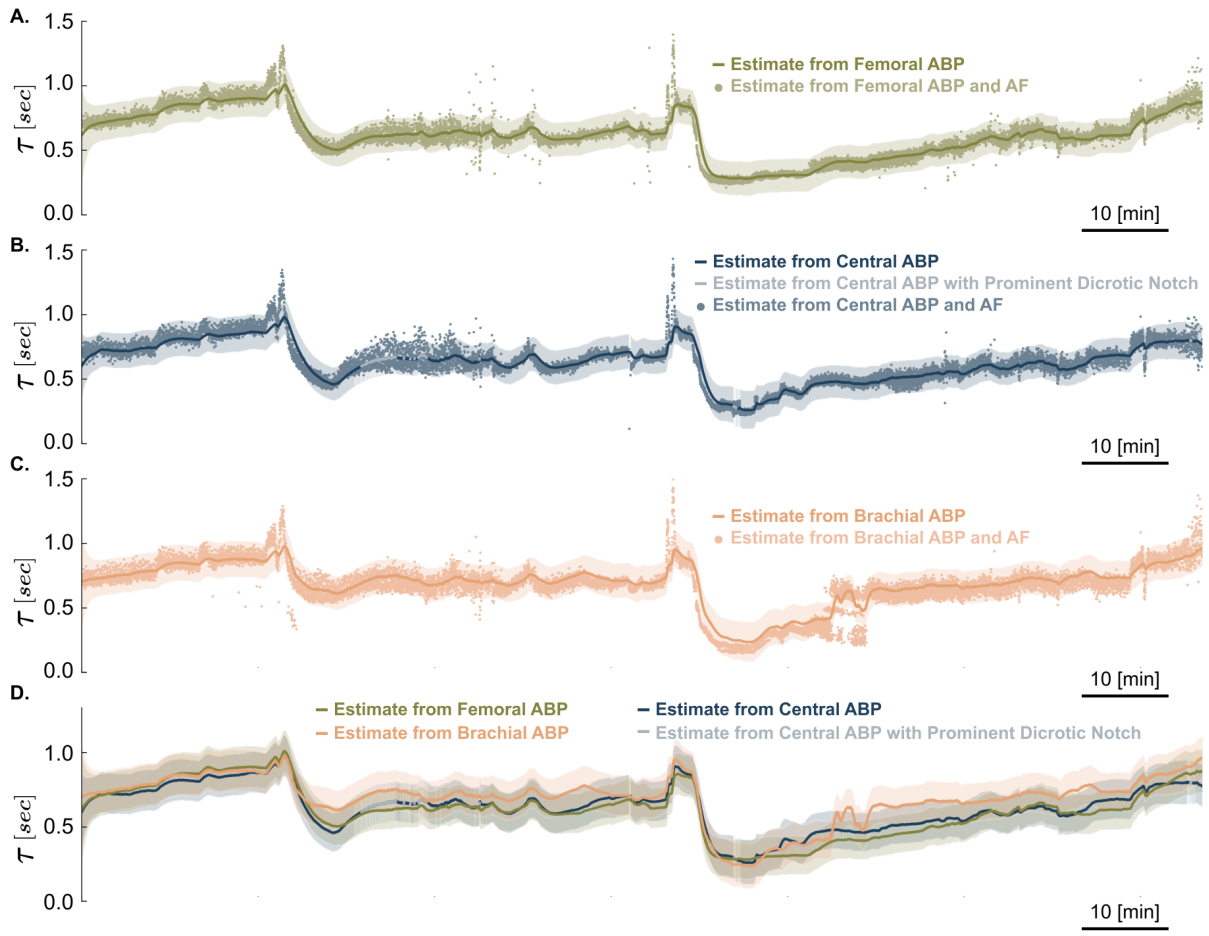

Fig. 5. **Experiment 1: Proportional R (τ) Estimation Results.** Accompanying each estimate using arterial blood pressure (ABP) is the calculated 95% credibility interval of τ_k at beat k. **A.** Comparison of the beat-by-beat estimate of τ using femoral ABP versus the beat-by-beat estimate of τ using femoral ABP and aortic flow. **B.** Same as A. but using central ABP. Areas of lighter blue indicate that the estimate using ABP was derived from a central ABP pulse with a prominent dicrotic notch. **C.** Same as A. but using brachial ABP. **D.** Agreement of our Kalman estimates using central, brachial or femoral ABP. Once again, areas of lighter blue indicate that the estimate using ABP was derived from a central ABP pulse with a prominent dicrotic notch.

estimates using three ABP recording locations: central, femoral and brachial. In every swine, we find that the estimates from ABP closely align with estimates derived using AF for central (Fig. 5A), femoral (Fig. 5B) and brachial (Fig. 5C) ABP recording locations. Summary statistics of these results are in Table I. We present full τ estimation results (Figs. S2-S6) and corresponding summary statistics for every experiment (Table S1) in the Supplementary Information.

TABLE I

SUMMARY STATISTICS OF ALIGNMENT BETWEEN ABP-DERIVED τ_p AND ABP-AF-DERIVED $\tau_{p,f}$ PROPORTIONAL R ESTIMATES AND BETWEEN τ_p FROM DIFFERENT CATHETER LOCATIONS (FEMORAL, BRACHIAL OR CENTRAL). WE PRESENT THE PEARSON CORRELATION COEFFICIENT, r, AVERAGE ABSOLUTE PERCENT ERROR, AAPE AND ROOT MEAN SQUARED ERROR NORMALIZED BY A MEAN OF THE DATA, $NRMSE_\mu$.

	r	AAPE	$NRMSE_\mu$
Femoral τ_p vs. $\tau_{p,f}$	.91	10 %	.14
Brachial τ_p vs. $\tau_{p,f}$	.89	17 %	.19
Central τ_p vs. $\tau_{p,f}$	.95	8 %	.11
Femoral vs. Central τ_p	.98	8 %	.08
Central vs. Brachial τ_p	.94	13%	.05
Femoral vs. Brachial τ_p	.93	16 %	.58

These experiments only measured flow into the aorta, not flow into the location of catheterization. To use this information for estimation with peripheral – femoral and brachial – ABP, we extended the two-element Windkessel model to incorporate different vascularization (Fig. S1). By assuming that the majority of arterial resistance comes from the microcirculation and each peripheral location of catheterization is prior to the microcirculation, the flow into the aorta can be used to estimate R and C from peripheral locations (see Supplementary Information, Sec. A).

F. Proportional resistance estimates derived from central and peripheral catheters align in multiple experiments

Clinically, it is desirable to estimate cardiovascular states peripherally to minimize invasiveness. To assess if τ can be estimated peripherally, we examined whether the brachial or femoral ABP-derived τ estimates agree with estimates derived from central ABP. Our prior analysis supports agreement of these estimates (Supplementary Information, Sec. A). We emphasize that the noise parameters of our Kalman filters were equivalent regardless of recording location.

In experiment 1, we find that the estimates derived from brachial, femoral and central ABP closely align (Fig. 5D). This alignment mostly extends to the remaining experiments (Figs. S2-S6). Specifically, we find that there is total alignment in 2 experiments (Figs. 5 and S5) and majority alignment in 2 additional experiments (Figs. S3 and S6). We present summary statistics of this result for experiment 1 (Table I) and for all experiments (Table S2) in the Supplementary Information.

In the remaining 2 experiments, there is a more prominent discrepancy between estimates derived from different locations (Figs. S2 and S4). We attribute these discrepancies to explicable morphological alterations in central ABP (see Supplementary Information, Sec. B) and measurement artifacts in peripheral ABP (see Supplementary Information, Sec. C). When there is presence of a prominent dicrotic notch in central ABP (Fig. S7), increased τ estimates as compared to peripheral ABP-derived estimates are observed. In experiment 4, the femoral ABP-derived estimates increase rapidly at about 8 minutes into the experiment most probably because of a bubble in the fluid-filled catheter or a similar artifact. This hypothesis is supported by analysis of a circuit modeling the impact of a bubble in a fluid-filled catheter (Fig. S8) and evidence presented in Figure S9.

G. Proportional resistance estimates enable estimation of proportional cardiac output

The time constant not only directly contains information about R, but also can be used to derive information about CO. Through use of the dynamic equation of the two-element Windkessel model (Eq. 1), we derived an estimate of proportional CO (CO/C) using either just ABP or AF and ABP. To derive our estimates of proportional CO using AF and ABP, we simply averaged AF over a pulse and divided this average by our estimates of C using ABP and AF. For estimates using just ABP, we used Eq. 4 with integration bounds over the full beat (i.e., from o_k to $o_k + T_k$) where each side of the equation was divided by T_k. We then solved for proportional CO at every beat using ABP measurements and ABP-derived τ estimates where CO_k is the average flow per beat k in $[\mathrm{L} \cdot \mathrm{min}^{-1}]$. The mathematical details of this method are provided in the Appendix.

We find that ABP-derived estimates of proportional CO closely align with estimates of proportional CO derived using highly invasive measurements of AF (Fig. 6A-C). Additionally, proportional CO estimates derived from brachial and femoral ABP agree with estimates derived from central ABP (Fig. 6D), as supported by previous analysis in the Supplementary Information, Sec. A. Summary statistics of these results are presented in Table II. We present full CO/C estimation results (Figs. S2-S6) and corresponding summary statistics for every experiment (Tables S3-S4) in the Supplementary Information.

H. Proportional resistance and cardiac output estimates change predictably in response to common cardiovascular drugs

As is emphasized in current clinical decision-making practices, changes in ABP are dependent on changes in cardiac function (captured by CO) and changes in vascular function (captured by R). Our prior results provide information of both cardiovascular states; more specifically, they can be viewed as proportional estimates of R (τ = RC) and CO (CO/C).

TABLE II

SUMMARY STATISTICS OF ALIGNMENT BETWEEN ABP-DERIVED $(\mathrm{CO/C})_p$ AND ABP-AF-DERIVED $(\mathrm{CO/C})_{p,f}$ PROPORTIONAL CO ESTIMATES AND BETWEEN $(\mathrm{CO/C})_p$ FROM DIFFERENT CATHETER LOCATIONS (FEMORAL, BRACHIAL OR CENTRAL). WE PRESENT THE PEARSON CORRELATION COEFFICIENT, r, AVERAGE ABSOLUTE PERCENT ERROR, AAPE AND ROOT MEAN SQUARED ERROR NORMALIZED BY A MEAN OF THE DATA, $NRMSE_\mu$.

	r	AAPE	NRMSE_μ
Femoral $(\mathrm{CO/C})_p$ vs. $(\mathrm{CO/C})_{p,f}$	.94	7 %	.11
Brachial $(\mathrm{CO/C})_p$ vs. $(\mathrm{CO/C})_{p,f}$	.79	13 %	.30
Central $(\mathrm{CO/C})_p$ vs. $(\mathrm{CO/C})_{p,f}$	.92	8 %	.11
Femoral vs. Central $(\mathrm{CO/C})_p$	.93	17 %	.22
Central vs. Brachial $(\mathrm{CO/C})_p$	.85	11%	.17
Femoral vs. Brachial $(\mathrm{CO/C})_p$	.88	23 %	.28

To further support clinical usefulness of these proportional estimates in pharmacological decision-making, we analyzed segments of their normalized changes in response to five drugs commonly used in clinical medicine: phenylephrine (PE), dobutamine (DB), esmolol (ES), nitroglycerin (NI) and fentanyl (FT). Our results provide evidence that changes in proportional R and CO estimates using ABP follow expected pharmacological effects of these drugs (Fig. 7). We additionally show every initiation of a drug for every experiment (Figs. S10-S15) with corresponding analyses in the Supplementary Information, Section D; these results hold, in general, across experiments and drugs.

Figure 7B exhibits the vasoconstrictive effects (increased R) of PE, an alpha-1 adrenergic agonist commonly used to increase ABP during states of vasodilation. Figure 7C shows the concomitant vasodilatory (decreased R) and positive inotropic effects (increased CO) of DB, a beta-1 and beta-2 adrenergic agonist commonly used to manage cardiogenic shock. In this case, the vasodilatory effects of DB overpower the vasoconstrictive effects of PE. Figure 7D showcases the concomitant vasoconstrictive effects (increased R) of PE along with the additional negative inotropic effects (decreased CO) of ES, a beta-1 adrenergic antagonist. The combined veno-arterial dilation effects of NI, a drug commonly used to treat hypertension and decrease myocardial oxygen demand, are shown in Figure 7E. Dilation of arteries decreases R and dilation of veins decreases return of blood volume to the heart, thus decreasing CO. Finally, the vasodilatory effects (decreased R) of boluses of FT, a mu-selective opioid agonist, are shown in Figure 7F.

III. DISCUSSION

Using the two-element Windkessel model, we have developed an approach to estimate changes in vascular function (R) and and cardiac function (CO) in real time. First, we developed a real-time method to estimate proportional R (τ = RC) from ABP. Second, we developed a method to estimate proportional CO (CO/C) from ABP and these proportional R estimates. Finally, using additional AF measurements, we developed a method to produce more-informed estimates of proportional R and CO. By

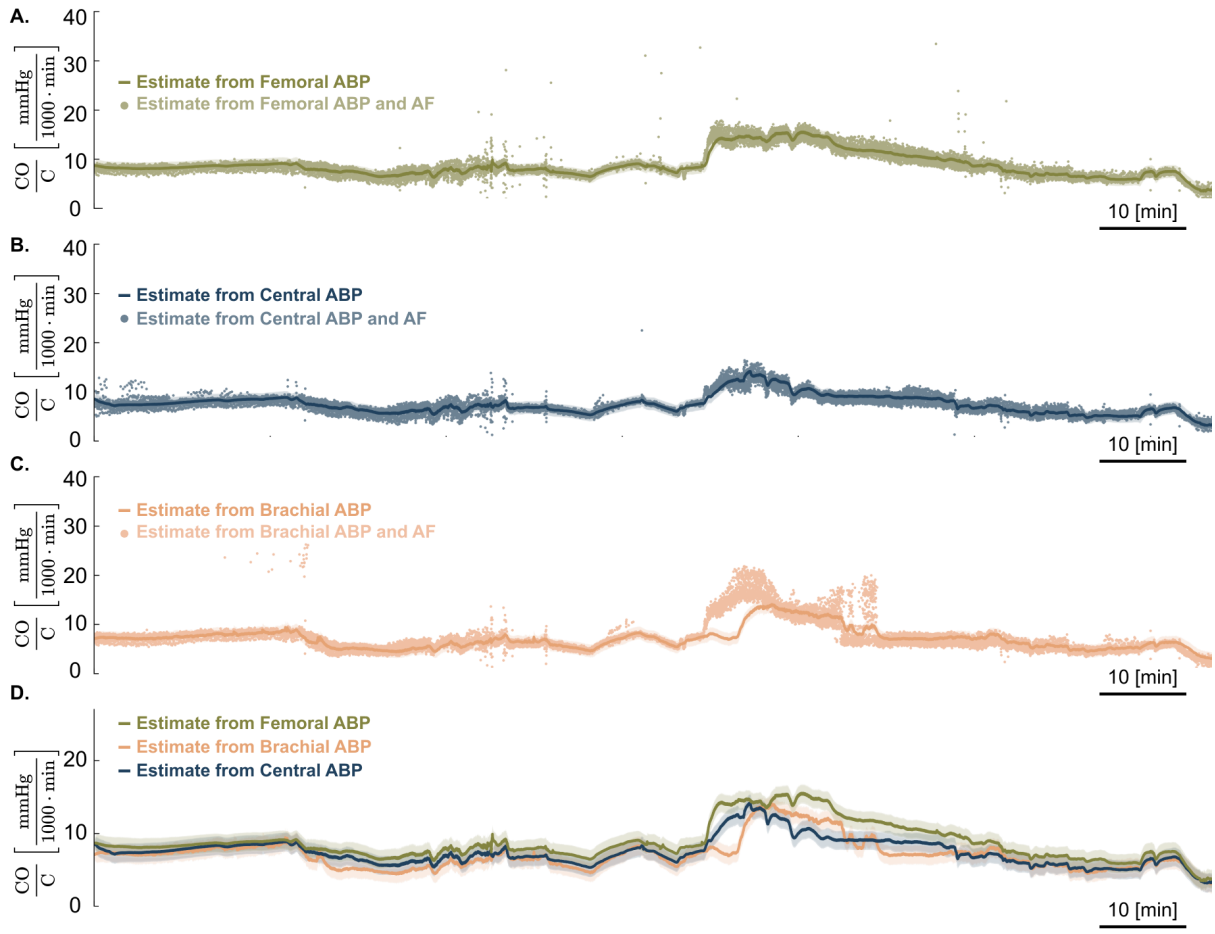

Fig. 6. **Experiment 1: Proportional CO (CO/C) Estimation Results.** Accompanying each estimate using arterial blood pressure (ABP) is the calculated 95% credibility interval of CO/C at beat k. **A.** Comparison of the beat-by-beat estimate of CO/C using femoral ABP and τ estimates versus the beat-by-beat estimate of CO/C using central ABP and aortic flow. **B.** Same as A. but using central ABP. **C.** Same as A. but using brachial ABP. **D.** Agreement of our Kalman estimates using central, brachial or femoral ABP with corresponding central, brachial or femoral τ estimates.

applying these methods to a previously collected swine dataset, we find that our proportional R and CO estimates from ABP not only closely align with estimates derived using AF, but also closely align when derived from various ABP recording locations. Additionally, we find that infusions of common often cardiovascular drugs affected these estimates predictably.

A. Interpretation of proportional R and CO

We have proposed states RC and CO/C for monitoring the cardiovascular system to guide clinical interventions that regulate ABP. To regulate ABP, a clinician must decide whether to use clinical interventions that primarily alter R or CO. We have found that common clinical drugs have distinct effects on RC and CO/C. With an ability to modulate both RC and CO/C, we have an ability to modulate the pressure waveform dynamics, as described by the dynamic equation of the Windkessel model (Eq. 1). With the simple assumption that pressure is equivalent at the beginning an end of a pulse, we get that mean arterial pressure (MAP) is RC · CO/C using the Windkessel model (see Supplementary Information, Sec. E). With this relation, by monitoring RC and CO/C and controlling each using common clinical interventions, we have complete control over MAP.

Our states can be contrasted with the states R and CO, which have immediate physiological relevance. Previous work has been proposed to estimate these reliably from minimally invasive ABP measurements. However, the Windkessel model informs us that this cannot be possible without additional information, like AF measurements (see Supplementary Information, Sec. F). Specifically, different values of R and CO can give us the same ABP pulse (Fig. S16). Alternatively, each ABP pulse can give us a unique value of RC and CO/C. As no drugs are clinically used to specifically alter C, it becomes uncertain how useful it is to estimate C for ABP regulation. Therefore, from a practical perspective, if we can only use minimally invasive ABP measurements, we believe that RC and CO/C are the states that should be estimated for reliable control of blood pressure intervention.

If additional measurements are performed, then we can certainly decompose RC and CO/C into R, C and CO. The separate estimation of these three variables can then help us address physiological questions, beyond intervention. For example, knowledge of a patient's compliance can indicate peripheral vascular diseases such as atherosclerosis, aneurysms, connective tissue diseases, synthetic vascular graft material and effects of aging. We plan to focus on separate estimation

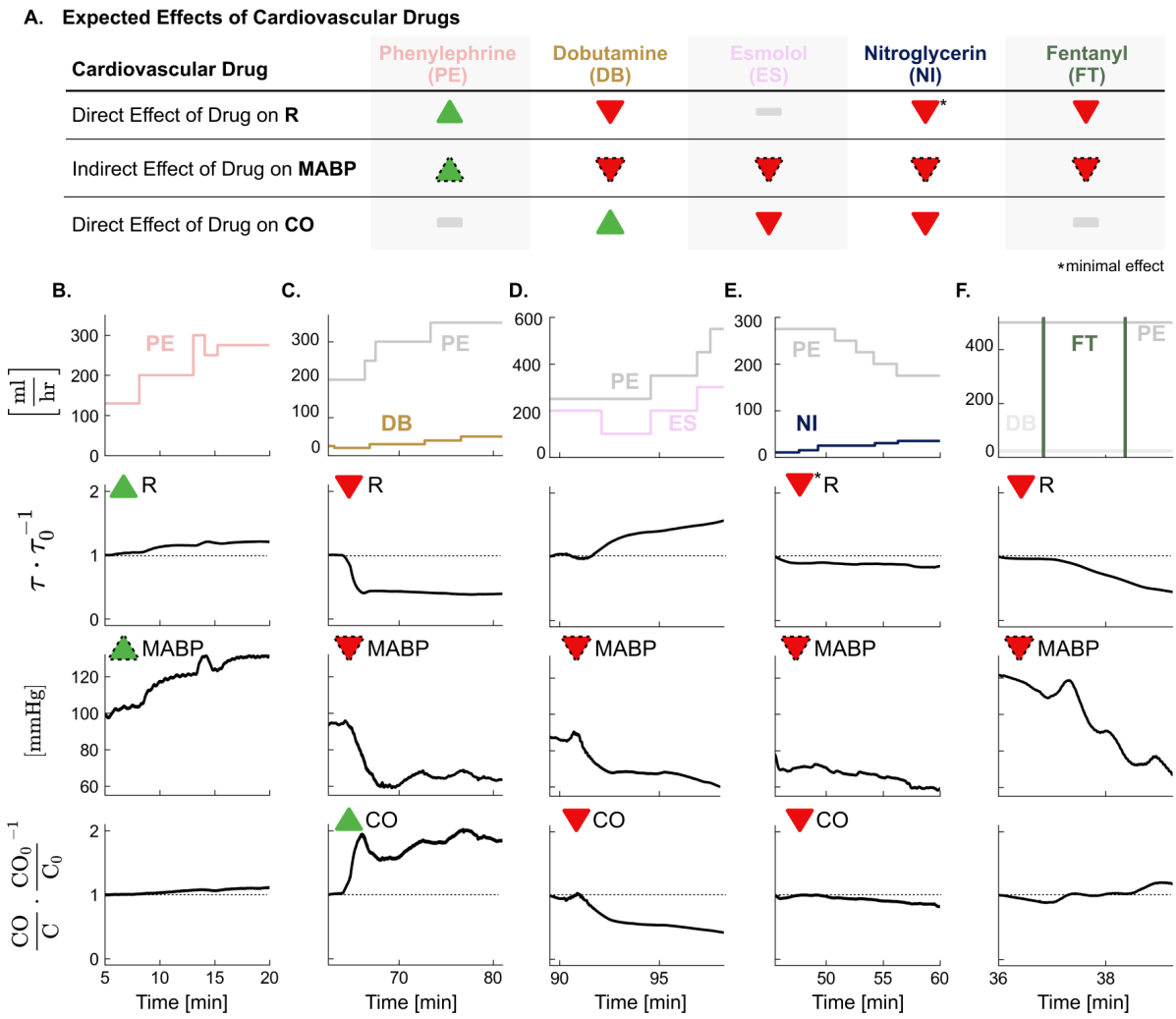

Fig. 7. **Effects of Common Cardiovascular Drugs on Femoral Mean Arterial Pressure (MAP) and Femoral ABP-derived Estimates of Proportional R and CO.** Here, k indexes the beat, and k_i indicates the initial beat of a segment. **A.** Direct (i.e., change in R or CO from change in drug concentrations) and indirect (i.e., change in MAP as a result of change in R or CO) effects of cardiovascular drugs phenylephrine (PE), dobutamine (DB), esmolol (ES), nitroglycerin (NI) and fentanyl (FT). Proportional R and CO estimates were normalized to the first estimate of the segment. **B.** Direct changes in estimates of τ and estimates of CO/C causing indirect changes in MAP from a PE infusion. Segment from Experiment 1. **C.** Same as B. but from a DB infusion with background PE. Segment from Experiment 3.**D.** Same as B. but from an ES infusion with background PE. Segment from Experiment 3. **E.** Same as B. but from an NI infusion with background PE. Segment from Experiment 5. **F.** Same as B. but from FT boluses with background DB and PE. Vertical lines indicate drug boluses. Segment from Experiment 6.

of R, C and CO in future work, comparing estimates with and without dynamic independence assumptions (Eqs. 2, 3, and 4) and exploring promising less invasive techniques for AF measurement, such as echocardiography [23], [29].

B. Methodological Benefits and Limitations

Our methods for proportional R and CO estimation using ABP yield beat-by-beat estimates with reduced noise and associated credibility intervals. For these reasons, our estimates greatly improve upon previous estimation methods using ABP and the two-element Windkessel model which either produce beat-by-beat estimates with significant noise [13] or estimates with reduced noise at minute time resolutions [14]–[16]. In these methods, we do not estimate C separately to provide direct estimates of R and CO. However, we have argued that RC (i.e., the rate of decay of pressure through the microcirculation) and CO/C (i.e., the rate of pressure increase from compliant arteries filling) are themselves useful and interpretable quantities.

Our method for proportional R and CO estimation using additional AF measurements relaxes a common and incorrect clinical assumption: that the R and C branches of the two-element Windkessel model both receive the full volume of aortic flow at each pulse [30]. For example, this assumption is explicitly used in Mukkamala et al. to derive proportional estimates of CO from τ [14]. Through relaxation of this assumption, our method extracts improved state estimates derived from ABP and AF. The resultant estimates do lack smoothness most likely because of varied alignment of AF and ABP pulses and because we did not implement a Kalman filter in this method. Given the reliability and clinical relevance of our estimates using ABP, improving this is not necessary.

C. Clinical Implications

The results from use of our approach have significant clinical implications. First, we have shown that we can estimate proportional R and CO with high accuracy from a single peripheral artery catheter. As such, clinical use of our approach may significantly decrease the need for use of high-risk interventions like pulmonary artery catheters. Peripheral artery catheters are already very commonly used in the OR and ICU settings and carry a very low complication rate in both adult [31] and pediatric [32] populations. Second, the consistency of our proportional R and CO estimates across the arterial tree – as supported by our extension of the two-element Windkessel model – show that these states are conserved throughout the arterial system. As such, clinicians could implement this approach using radial or femoral peripheral artery catheters. Third, the predictable responses of these states to standard cardiovascular drugs emphasize the actionable information about changing vascular and cardiac function contained in our estimates. In general, our approach enables clinicians to accurately track these vital hemodynamic states throughout the perioperative period and during critical illness with peripheral artery catheters. In severe patient cases, our estimates can provide guidance to clinicians during the transition to techniques using highly invasive measurements when necessary. In addition to their immediate clinical relevance, our proportional R and CO estimates can inform pharmacodynamic studies or function as controllable signals for a closed-loop system for cardiovascular control [33], [34]. We emphasize that prior to integration in clinical care, extensive analyses of this technique using larger datasets from both swine and human subjects is necessary; we will pursue this in future work.

IV. Conclusion

We developed a novel state-space approach for real-time proportional estimation of systemic vascular resistance and cardiac output. We then validated this approach with a previously collected swine cardiovascular dataset. Specifically, we showed that reliable estimates of a dynamic time constant of the two-element Windkessel model enabled reliable estimation of proportional systemic vascular resistance and cardiac output. We developed methods which estimate proportional resistance and cardiac output from arterial blood pressure measurements and estimate resistance and cardiac output directly with both arterial blood pressure and aortic flow measurements. Through use of a Kalman filter, our arterial blood pressure-derived estimates are beat-by-beat with reduced noise. Regardless of the arterial catheter location, we found that our arterial blood pressure-derived estimates closely align with those from both arterial blood pressure and aortic flow and with each other. Even further, our proportional resistance and cardiac output estimates often change predictably in response to common cardiovascular drugs.

This work addresses a difficult decision clinicians face daily when managing blood pressure: is this patient hypotensive or hypertensive because of changes in vascular tone (i.e., systemic vascular resistance) or blood flow out of the heart (i.e., cardiac output)? Clinicians must differentiate these causes of arterial blood pressure changes to ensure that treatment appropriately restores end-organ perfusion and does not cause inadvertent complications. Estimates of resistance and cardiac output from our approach provide information that can readily be used to guide hemodynamic management decisions in real time. Even further, estimates from our approach can also be used in pharmacodynamic studies to delineate effects of a drug on different components of the cardiovascular system or can serve as a control signal for use in closed-loop systems for cardiovascular control (e.g., closed-loop control of blood pressure).

Appendix: Materials and Methods

A. Experimental data

We used a previously collected swine dataset [14] with which we applied our estimation approach. In this dataset, the cardiovascular systems of six young Yorkshire swine (30–34 [kg]) were monitored while under isoflurane anesthesia. In each experiment, recordings were made of peripheral ABP (femoral and brachial), central ABP and AF. An external pressure transducer (TSD104A, Biopac Systems, Santa Barbara, CA) was used for femoral ABP, a 23- or 25-gauge angiocatheter was placed as distal as possible to the brachial artery for brachial ABP and a micro-manometer-tipped catheter (SPC 350, Millar Instruments, Houston, TX) was fed retrograde to the thoracic aorta for central ABP. The central catheter was placed such that ABP pulse decays resembled an exponential decay. AF was recorded from an ultrasonic flow probe (T206 with A-series probes, Transonic Systems, Ithaca, NY) placed around the aortic root [14]. This protocol yielded ABP and AF both sampled at 250 [Hz].

A wide array of drugs were used to manipulate the cardiovascular system including the following: phenylephrine (PE), dobutamine (DB), esmolol (ES), nitroglycerin (NI) and fentanyl (FT). These drugs each have varied mechanisms of action. PE increases R as an alpha-1 adrenergic agonist [35] and has been shown to have varied indirect effects on CO [36]–[38]. DB increases cardiac output as a beta-1 adrenergic agonist and decreases R as a beta-2 adrenergic agonist [39]. ES decreases CO as a beta-1 adrenergic antagonist [40] and can sometimes increase R through beta-2 antagonism at high doses [41]. NI generates nitric oxide which relaxes smooth muscles. Its effect is most prominent in the veins, which decreases cardiac preload and CO as a result. It minimally decreases R, which represents resistance in the arteries [42]. FT decreases R as a mu-selective opioid agonist [43], [44]. Additional drugs used in these experiments (acetylcholine and isoprotenerol) are presented in the Supplementary Information.

B. Arterial blood pressure and aortic flow signal processing

We describe the ABP and AF signal processing necessary to implement our estimation methods. This required identification of the onset, systolic peak and end of systole (beginning of diastole) for each ABP pulse. For central ABP, we also identified prevalent dicrotic notches, as described in the Supplementary Information. Finally, for our methods using highly invasive measurements, we corrected alignment of each AF and ABP pulse.

We first filtered each ABP waveform, $p[n]$, using a Kaiser window low pass filter with a pass band at 10 [Hz] and a stop band at 12 [Hz]. We then defined a first-order backwards difference approximation, $p_d[n]$, to the first derivative of pressure, $\dot{p}(t)$:

$$p_d[n] \coloneqq \frac{p(nT_s) - p(nT_s - T_s)}{T_s} \tag{7}$$

where $T_s = 60 f_s^{-1}$ is the sampling period of $p[n]$.

Next, we did initial detection of the ABP pulse onsets using the slope sum technique [45], with experiment-specific thresholds. Using insight from the two-element Windkessel model, we identified the onset of an ABP pulse to be when the derivative of p begins to increase after the diastolic decay. As such, we corrected our onsets to be the first minimum of $p_d[n]$ looking backwards from the detected onset from the slope sum technique.

Following our onset detection, we found the systolic peak with a simple maximum of $p[n]$ between the onset of beat k and $k+1$. We then identified the approximate end of systole, the point when the aortic valve closes, as the first minimum of $p_d[n]$ following the systolic peak. This point was chosen because, following an aortic flow pulse, there is a period of backflow as the aortic valve closes. This is visible at $t \approx .22$ [sec] in Fig. 2B. When simulating the two-element Windkessel model with a swine AF pulse, this backflow leads to a maximum rate of decay in the simulated pressure, hence the selection of a local minimum of $p_d[n]$.

Finally, for the methods using AF, we implemented a procedure to align AF pulses with ABP pulses. We defined correct pulse alignment as when, for pulse k, the point of greatest backflow of $f[n]$ (the minimum of $f[n]$) aligns with the minimum in $p_d[n]$ following the systolic peak. This approach uses similar logic to our approach for identification of the end of diastole of an ABP pulse. If the calculated shift suggested to shift the AF pulse backwards in time, we then corrected the AF shift to the previous beat's shift. We implemented this correction because central, femoral or brachial ABP pulses must be delayed in time compared to the AF pulse (a blood flow pulse out of the heart passes through the aorta before reaching either location of catheterization).

These detected ABP and AF features are all necessary to run our estimation methods using ABP yielding estimates of proportional R and CO and our estimation method using ABP and AF yielding direct estimates of R, C and CO.

C. Physiological model

We used the two-element Windkessel model [19] as the underpinning of our estimation methods using ABP or ABP and AF with additional assumptions that the model parameters, R, C and CO, are time-varying and that there is a single parameter value at every beat, k. The model is explored in more detail in the Section II-A.

D. Estimation of proportional R (τ) from aortic flow and arterial blood pressure

Using ABP and AF, we developed a method to estimate τ by separately estimating R and C to get $\tau = RC$. Substituting Equation 7 into Equation 1, with our assumption that R and C vary between beats led to:

$$f[n] = \frac{1}{R_k} p[n] + C_k p_d[n] \text{ for } t \text{ within beat } k \tag{8}$$

We then did a simple numerical integration using the rectangular rule to both sides over integration period n_0 to n_1:

$$\sum_{n_0}^{n_1} f[n] T_s = \frac{1}{R_k} \sum_{n_0}^{n_1} p[n] T_s + C_k \sum_{n_0}^{n_1} p_d[n] T_s \tag{9}$$

We selected two unique integration periods: the systolic period and the full beat. We skipped pulses where the ABP-AF alignment procedure failed (i.e., pulse segments were empty vectors). By choosing two unique integration periods, we then had two equations with two unknowns and could solve for an estimate of R_k and C_k separately. We first solved for C_k using the systolic segment and then R_k using C_k and the full beat. These R_k and C_k estimates then yielded an estimate of τ_k.

E. Estimation of proportional R (τ) from arterial blood pressure

We developed a state-space model of τ_k, the time constant parameter in the two-element Windkessel model at beat k, where the state equation is a Gaussian random walk and the observation equation relates samples of the diastolic portion of an ABP pulse to the slowly varying τ_k. With this state-space model, we estimated τ_k using a Kalman Filter.

We began with the observation equation. From the two-element Windkessel model, we can describe the diastolic decay of an ABP pulse in terms of τ_k. The ABP waveform follows an exponential decay beginning at the end of the systolic period, following the inflow of ΔV_k [L] of blood volume into the system. So, for a particular beat, we specified the following relationship between τ_k and a single sample of the diastolic portion of the blood pressure waveform, $v_{k,i}$:

$$v_{k,i} = a_k \exp\left(-\frac{t_{k,i}}{\tau_k}\right) \tag{10}$$

where k indexes the heart beats and i indexes the I_k observations per beat taken at a sampling rate f_s in [Hz]. The number of observations per time point vary for each beat: hence, I is also indexed by k. Additionally, $t_{k,i}$ corresponds to the time value in [sec] elapsed from the first blood pressure observation, $y_{k,0}$, and a_k is the y-intercept of the exponential function at $t_{k,0}$. We assumed a_k to be the initial observation of the diastolic period, $v_{k,i}$. Full observation vectors at pulse k were removed if expected to be faulty (e.g., if $I_k > 1.5 I_{k-1}$, $I_k < .5 I_{k-1}$ or if the first sample was less than the final sample). For simplicity, we then log-transformed equation (10):

$$\log(v_{k,i}) = \log(a_k e^{-\frac{t_{k,i}}{\tau_k}}) \tag{11}$$

$$= \log(a_k) - \frac{1}{\tau_k} t_{k,i} \tag{12}$$

Next we defined:

$$w_{k,i} \coloneqq -(\log(v_{k,i}) - \log(a_k)) \tag{13}$$

where any $w_{k,i} = 0$ was removed. Then, we solved for an equation relating the underlying τ_k to our observations (ratio of amount of time passed from the initial observation, $t_{k,i}$, to the pressure drop, w_k) and made the assumption that our observations were noisy:

$$\frac{t_{k,i}}{w_{k,i}} = \tau_k + \epsilon_{k,i} \tag{14}$$

where each $\epsilon_{k,i} \sim N(0, \sigma^2_{\epsilon,k,i})$. We assumed increasing confidence in observations later in the beat (i.e., $\sigma^2_{\epsilon,k,i}$ decreases with increasing i).

We now define $y_{k,i} \coloneqq t_{k,i} \cdot w^{-1}_{k,i}$. We removed any $y_{k,i}$ that was not in a physiological range for τ_k (e.g., $8 > y_k > .2$). With these definitions, we have our full observation equation. Our observation equation can be written in a more compact notation by expanding over the i index. We do not include $i = 0$, because this observation gives us no additional information. This is our final observation equation:

$$\begin{bmatrix} y_{k,1} \\ y_{k,2} \\ \vdots \\ y_{k,I_k-1} \end{bmatrix} = \begin{bmatrix} 1 \\ 1 \\ \vdots \\ 1 \end{bmatrix} \tau_k + \begin{bmatrix} \epsilon_{k,1} \\ \epsilon_{k,2} \\ \vdots \\ \epsilon_{k,I_k-1} \end{bmatrix} \tag{15}$$

Equation 15 can be represented in the following way:

$$\mathbf{y}_k = \mathbf{1}_k \tau_k + \boldsymbol{\epsilon}_k \tag{16}$$

where we have column vectors $\mathbf{y}_k \in \mathbb{R}^{I_k-1}$, $\tau_k \in \mathbb{R}$, $\boldsymbol{\epsilon}_k \in \mathbb{R}^{I_k-1}$ and $\mathbf{1}_k$ is a vector of ones with length $I_k - 1$. The covariance matrix of the defined noise vector at beat k is $\boldsymbol{\Sigma}_{\boldsymbol{\epsilon},k} = \text{diag}(\sigma^2_{\epsilon,k,i})$ of dimension $I_k - 1 \times I_k - 1$.

We then specified a state-space equation which simply constrains the state values to vary smoothly over time, as we don't expect the cardiovascular state, τ_k, to change rapidly. As such, we assumed τ_k follows a Gaussian random walk:

$$\tau_{k+1} = \tau_k + \eta_k \tag{17}$$

where $\eta_k \sim N\left(0, \sigma^2_\eta\right)$ and each η_k is independent.

We then used a Kalman Filter to estimate τ_k given our above state-space model. Given a maximum a posteriori (MAP) estimate, $\tau_{[k-1|k-1]}$, of τ_{k-1} at beat $k-1$ and our defined observation and state equations with Gaussian additive noise, we could fully specify our state estimation method using the traditional Kalman filter equations.

First, we defined our one-step prediction density. We specified this Gaussian distribution with the one-step state prediction of τ_k for beat k given observations up to beat $k-1$:

$$\tau_{[k|k-1]} = \tau_{[k-1|k-1]} \tag{18}$$

and the following one-step prediction variance as:

$$\sigma^2_{[k|k-1]} = \sigma^2_{[k-1|k-1]} + \sigma^2_\eta \tag{19}$$

Next, we defined our Kalman gain term:

$$\mathbf{K}_k = \sigma^2_{[k|k-1]} \mathbf{1}_k^T (\mathbf{1}_k \sigma^2_{[k|k-1]} \mathbf{1}_k^T + \boldsymbol{\Sigma}_{\boldsymbol{\epsilon},k})^{-1} \tag{20}$$

We specified our posterior density, additionally a Gaussian distribution, with the MAP estimate at beat k given observations including beat k as:

$$\tau_{[k|k]} = \tau_{[k|k-1]} + \mathbf{K}_k (\mathbf{y}_k - \mathbf{1}_k \tau_{[k|k-1]}) \tag{21}$$

and our posterior density variance as:

$$\sigma^2_{[k|k]} = (1 - \mathbf{K}_k \mathbf{1}_k) \sigma^2_{k|k-1} (1 - \mathbf{K}_k \mathbf{1}_k)^T + \mathbf{K}_k \boldsymbol{\Sigma}_{\boldsymbol{\epsilon},k} \mathbf{K}_k^T \tag{22}$$

In order to run this Kalman filter, we made an assumption of the distribution of the initial state, τ_0. The following observation equation corresponds to this beat:

$$\mathbf{y}_0 = \mathbf{1}_0 \tau_0 + \boldsymbol{\epsilon}_0 \tag{23}$$

We defined the MAP estimate, $\tau_{[0|0]}$, with a standard linear regression which defines the MAP estimate as:

$$\tau_{[0|0]} = \left(\mathbf{1}_0^T \mathbf{1}_0\right)^{-1} \mathbf{1}_0^T \mathbf{y}_0 \tag{24}$$

with variance:

$$\sigma^2_{[0|0]} = \left(\mathbf{1}_0^T \mathbf{1}_0\right)^{-1} \hat{\sigma}^2_\epsilon \tag{25}$$

and a further specified:

$$\hat{\sigma}^2_\epsilon = \frac{(\mathbf{y}_0 - \mathbf{1}_0 \tau_{[0|0]})^T (\mathbf{y}_0 - \mathbf{1}_0 \tau_{[0|0]})}{I_0} \tag{26}$$

where, recall that I_0 is the number of observations from the initial beat. With this specified Kalman filter, a MAP estimate, $\tau_{[k|k]}$, can be obtained for every beat. Additionally, a 95% credibility interval, the analog to a confidence interval in Bayesian statistics, can be calculated for each $\tau_k \sim N(\tau_{[k|k]}, \sigma^2_{[k|k]})$ by generating the cumulative distribution function of τ_k and finding the 2.5th and 97.5th percentiles.

F. Estimation of proportional CO using proportional R estimates

With AF and ABP, we estimated CO/C. We did this by averaging $f[n]$ over each pulse and dividing that by estimates of C_k calculated using AF and ABP.

With ABP, we additionally estimated CO/C using Equation 8 and τ estimates. To do this, we averaged over the full beat from the onset of pulse k (at sample o_k) to the following onset (at sample o_{k+1}):

$$\frac{1}{N_k} \sum_{o_k}^{o_{k+1}} \frac{1}{\tau_{[k|k]}} p[n] T_s + p_d[n] T_s = \frac{1}{\text{C}_k N_k} \sum_{o_k}^{o_{k+1}} f[n] T_s \tag{27}$$

where N_k is the number of samples for the full pulse, k, and CO is average flow per pulse. We additional made the assumption that following the detected systolic end of $p[n]$, flow was zero. This provided a single observation of CO/C for every beat. We then implemented a Gaussian Kalman Filter using this single observation per beat to produce smooth estimates of $(\text{CO/C})_k$.

G. Summary statistics of estimation performance

We selected the following summary statistics to further analyze the performance of our estimation frameworks: the Pearson product-moment correlation coefficient, average absolute percent error, and root mean square error normalized by a mean of the data. Details of our explicit formulations are in the Supplementary Information, Section G.

ACKNOWLEDGMENTS

We acknowledge Dr. Ramakrishna Mukkamala for sharing the swine dataset used in this work.

REFERENCES

[1] S. Aronson, M. Stafford-Smith, B. Phillips-Bute, A. Shaw, J. Gaca, and M. Newman, "Intraoperative systolic blood pressure variability predicts 30-day mortality in aortocoronary bypass surgery patients," *Anesthesiology*, vol. 113, pp. 305–12, August 2010.

[2] M. Walsh, P. J. Devereaux, A. X. Garg, A. Kurz, A. Turan, R. N. Rodseth, J. Cywinski, L. Thabane, and D. I. Sessler, "Relationship between intraoperative mean arterial pressure and clinical outcomes after noncardiac surgery: Toward an empirical definition of hypotension," *Anesthesiology*, vol. 119, pp. 507–15, September 2013.

[3] E. Futier, J.-Y. Lefrant, P.-G. Guinot, T. Godet, E. Lorne, P. Cuvillon, S. Bertran, M. Leone, B. Pastene, V. Piriou, S. Molliex, J. Albanese, J.-M. Julia, B. Tavernier, E. Imhoff, J.-E. Bazin, J.-M. Constantin, B. Pereira, and S. Jaber, "Effect of individualized vs standard blood pressure management strategies on postoperative organ dysfunction among high-risk patients undergoing major surgery: A randomized clinical trial," *JAMA*, vol. 318, no. 14, pp. 1346–1357, 2017.

[4] E. Wesselink, T. Kappen, H. Torn, A. Slooter, and W. van Klei, "Intraoperative hypotension and the risk of postoperative adverse outcomes: a systematic review," *British Journal of Anaesthesia*, vol. 121, no. 4, pp. 706–721, 2018.

[5] J. Varon and P. E. Marik, "Perioperative hypertension management," *Vascular health and risk management*, vol. 4, no. 3, pp. 615–627, 2008.

[6] L. Lonjaret, O. Lairez, V. Minville, and T. Geeraerts, "Optimal perioperative management of arterial blood pressure," *Integrated blood pressure control*, pp. 49–59, 2014.

[7] L. Meng, W. Yu, T. Wang, L. Zhang, P. M. Heerdt, and A. W. Gelb, "Blood pressure targets in perioperative care: provisional considerations based on a comprehensive literature review," *Hypertension*, vol. 72, no. 4, pp. 806–817, 2018.

[8] B. Saugel, K. Kouz, A. S. Meidert, L. Schulte-Uentrop, and S. Romagnoli, "How to measure blood pressure using an arterial catheter: a systematic 5-step approach," *Critical care (London, England)*, vol. 24, p. 172, Apr 2020.

[9] I. T. Bootsma, E. C. Boerma, T. W. L. Scheeren, and F. de Lange, "The contemporary pulmonary artery catheter. part 2: measurements, limitations, and clinical applications," *Journal of Clinical Monitoring and Computing*, vol. 36, no. 1, pp. 17–31, 2022.

[10] J. R. Navas-Blanco, A. Vaidyanathan, P. T. Blanco, and R. K. Modak, "CON: Pulmonary artery catheter use should be forgone in modern clinical practice," *Ann Card Anaesth*, vol. 24, pp. 8–11, Jan. 2021.

[11] M. R. Shah, C. M. O'Connor, G. Sopko, V. Hasselblad, R. M. Califf, and L. W. Stevenson, "Evaluation study of congestive heart failure and pulmonary artery catheterization effectiveness (ESCAPE): Design and rationale," *American Heart Journal*, vol. 141, no. 4, pp. 528–535, 2001.

[12] S. Viviani, "Pulmonary-Artery versus Central Venous Catheter to Guide Treatment of Acute Lung Injury," *New England Journal of Medicine*, vol. 365, pp. 687–696, 2011.

[13] A. C. Simon, M. E. Safar, J. A. Levenson, G. M. London, B. I. Levy, and N. P. Chau, "An evaluation of large arteries compliance in man," *American Journal of Physiology-Heart and Circulatory Physiology*, vol. 237, no. 5, pp. H550–H554, 1979. PMID: 495760.

[14] R. Mukkamala, A. T. Reisner, H. M. Hojman, R. G. Mark, and R. J. Cohen, "Continuous cardiac output monitoring by peripheral blood pressure waveform analysis.," *IEEE Transactions on Biomedical Engineering*, vol. 53, pp. 459–67, Mar 2006.

[15] T. Parlikar, T. Heldt, G. Ranade, and G. Verghese, "Model-based estimation of cardiac output and total peripheral resistance," in *2007 Computers in Cardiology*, pp. 379–382, 2007.

[16] N. Fazeli and J.-O. Hahn, "Estimation of cardiac output and peripheral resistance using square-wave-approximated aortic flow signal," *Frontiers in Physiology*, vol. 3, 2012.

[17] W. Yin, A. Tivay, and J.-O. Hahn, "Hemodynamic monitoring via model-based extended kalman filtering: Hemorrhage resuscitation and sedation case study," in *2022 American Control Conference (ACC)*, pp. 3352–3352, 2022.

[18] A. Tivay and J.-O. Hahn, "A population-informed particle filter for robust physiological monitoring using low-information time-series measurements," *IEEE Transactions on Biomedical Engineering*, vol. 70, no. 8, pp. 2298–2309, 2023.

[19] O. Frank, "Die grundform des arteriellen pulses," *Zeitschrift fur Biologie*, vol. 37, p. 483–526, 1899.

[20] P. J. Peyton and S. W. Chong, "Minimally Invasive Measurement of Cardiac Output during Surgery and Critical Care: A Meta-analysis of Accuracy and Precision," *Anesthesiology*, vol. 113, pp. 1220–1235, 11 2010.

[21] A. Joosten, O. Desebbe, K. Suehiro, L. S.-L. Murphy, M. Essiet, B. Alexander, M.-O. Fischer, L. Barvais, L. Van Obbergh, D. Maucort-Boulch, and M. Cannesson, "Accuracy and precision of non-invasive cardiac output monitoring devices in perioperative medicine: a systematic review and meta-analysisÄ†," *BJA: British Journal of Anaesthesia*, vol. 118, pp. 298–310, 02 2017.

[22] M. Hadian, H. K. Kim, D. A. Severyn, and M. R. Pinsky, "Cross-comparison of cardiac output trending accuracy of LiDCO, PiCCO, FloTrac and pulmonary artery catheters," *Crit Care*, vol. 14, p. R212, Nov. 2010.

[23] J. Kobe, N. Mishra, V. K. Arya, W. Al-Moustadi, W. Nates, and B. Kumar, "Cardiac output monitoring: Technology and choice," *Annals of Cardiac Anaesthesia*, vol. 22, pp. 6–17, Jan 2019.

[24] "Figure graphic created with biorender."

[25] R. G. Mark, "Cardiovascular mechanics; quantitative physiology: Organ transport systems," 2004.

[26] B. E. Westerhof, I. Guelen, N. Westerhof, J. M. Karemaker, and A. Avolio, "Quantification of wave reflection in the human aorta from pressure alone: a proof of principle," *Hypertension*, vol. 48, no. 4, pp. 595–601, 2006.

[27] W. Nichols, M. F. O'Rourke, and C. Vlachopoulos, *McDonald's Blood Flow in Arteries: Theoretical, Experimental and Clinical Principles (Sixth Edition)*. Hodder Education Publishers, 2011.

[28] C. Russo, Z. Jin, Y. Takei, T. Hasegawa, S. Koshaka, V. Palmieri, M. S. Elkind, S. Homma, R. L. Sacco, and M. R. D. Tullio, "Arterial wave reflection and subclinical left ventricular systolic dysfunction," *Journal of Hypertension*, vol. 29, no. 3, pp. 574–582, 2011. Research Support, N.I.H., Extramural.

[29] Y. Zhang, Y. Wang, J. Shi, Z. Hua, and J. Xu, "Cardiac output measurements via echocardiography versus thermodilution: A systematic review and meta-analysis," *PLoS One*, vol. 14, p. e0222105, 10 2019.

[30] J. Trammel and A. Sapra, "Physiology, systemic vascular resistance." Internet, Jul 10 2023. Updated on 2023 Jul 10.

[31] B. Scheer, A. Perel, and U. J. Pfeiffer, "Clinical review: complications and risk factors of peripheral arterial catheters used for haemodynamic monitoring in anaesthesia and intensive care medicine," *Crit Care*, vol. 6, pp. 199–204, Apr. 2002.

[32] S. J. Gleich, A. V. Wong, K. S. Handlogten, D. E. Thum, and M. E. Nemergut, "Major short-term complications of arterial cannulation for monitoring in children," *Anesthesiology*, vol. 134, pp. 26–34, Jan. 2021.

[33] T. E. Baum and E. N. Brown, "Theoretical development of a closed-loop system for blood pressure control," in *2021 American Control Conference (ACC)*, pp. 672–677, 2021.

[34] T. E. Baum, B. Satchidanandan, M. A. Dahleh, and E. N. Brown, "A study of robustness of a closed-loop system for blood pressure control," in *2023 American Control Conference (ACC)*, pp. 2879–2886, 2023.

[35] J. H. Hengstmann and J. Goronzy, "Pharmacokinetics of ^{3}H-phenylephrine in man," *European Journal of Clinical Pharmacology*, vol. 21, no. 4, pp. 335–341, 1982.

[36] M. Cannesson, Z. Jian, G. Chen, T. Q. Vu, and F. Hatib, "Effects of phenylephrine on cardiac output and venous return depend on the position of the heart on the frank-starling relationship," *Journal of applied physiology*, vol. 113, no. 2, pp. 281–289, 2012.

[37] O. Rebet, O. Andremont, J.-L. Gerard, J.-L. Fellahi, J.-L. Hanouz, and M.-O. Fischer, "Preload dependency determines the effects of phenylephrine on cardiac output in anaesthetised patients: a prospective observational study," *European Journal of Anaesthesiology— EJA*, vol. 33, no. 9, pp. 638–644, 2016.

[38] A. Kalmar, S. Allaert, P. Pletinckx, J.-W. Maes, J. Heerman, J. Vos, M. Struys, and T. Scheeren, "Phenylephrine increases cardiac output by raising cardiac preload in patients with anesthesia induced hypotension," *Journal of clinical monitoring and computing*, vol. 32, pp. 969–976, 2018.

[39] H. C. Hemmings and T. D. Egan, *Pharmacology and physiology for anesthesia e-book: foundations and clinical application*. Elsevier Health Sciences, 2012.

[40] J. Askenazi, P. E. MacCosbe, J. Hoff, P. Turlapaty, T. A. Hua, and A. Laddu, "Hemodynamic effects of esmolol, an ultrashort-acting beta blocker," *The Journal of Clinical Pharmacology*, vol. 27, no. 8, pp. 567–573, 1987.

[41] A. Pevtsov, C. Kerndt, I. Ahmed, *et al.*, "Esmolol." https://www.ncbi.nlm.nih.gov/books/NBK518965/, 2024. Updated 2024 Jan 30.

[42] D. Williams, E. Amsterdam, and D. Mason, "Hemodynamic effects of nitroglycerin in acute myocardial infarction.," *Circulation*, vol. 51, no. 3, pp. 421–427, 1975.
[43] G. M. Bennett and T. H. Stanley, "Cardiovascular effects of fentanyl during enflurane anesthesia in man," *Anesthesia & Analgesia*, vol. 58, no. 3, pp. 179–182, 1979.
[44] C. C. Hug, Jr, "Opioids: clinical use as anesthetic agents," *J Pain Symptom Manage*, vol. 7, pp. 350–355, Aug. 1992.
[45] W. Zong, T. Heldt, G. Moody, and R. Mark, "An open-source algorithm to detect onset of arterial blood pressure pulses," in *Computers in Cardiology, 2003*, pp. 259–262, 2003.